On the Effects of Design Parameters on Quadruped Robot Gaits

Dimitrios Myrisiotis, Ioannis Poulakakis, *Member, IEEE* and Evangelos Papadopoulos, *Senior Member, IEEE**

***Abstract*—In this work, we link the various parameters that characterize a quadruped robot to the gait that it eventually opts for the steady state part of its locomotion. We then introduce an appropriate class of motion patterns, and provide some evidence that certain parameter values tend to favor specific pattern subclasses. This offers a new robot walking behavior qualitative view and some novel guidelines for legged systems design, in regard to the gait-effects of each design parameter. To accomplish the above, we adopt the use of an underactuated quadruped robot, and the Hildebrand diagrams paradigm for the succinct portraiture of its gaits, as well as the use of two distinct definitions regarding the motion stride.**

I. Introduction

In the past years, a large number of research activities have taken place in regard to legged robots. This is mainly due to the advantages legged robots have in unstructured or unprepared terrains, in comparison to wheeled locomotion [1], [2]. A great number of these activities concern quadruped robots, since they achieve a good trade-off between performance and design and control complexity.

Many interesting quadruped legged robots have been developed, including the BigDog and Cheetah of Boston Dynamics, which are able to perform a number of different tasks [3]. The way quadruped robots locomote affects many aspects of their function, like energy efficiency, dynamic stability and disturbance robustness. Thus, it is important to be able to describe concisely the way a quadruped robot moves. *But how can one achieve this?* One of the possible ways, is the Hildebrand diagram [4]. Another way to do this are the support sequences of Muybridge [5], [4]. Both of these techniques were first used in Biology, for the portaiture of the gaits of legged animals.

In this paper, we consider the problem of characterizing the impact the various quadruped robot parameters can carry on its locomotion behavior. To do this, (a) we employ two different robot models which differ in the existence of leg mass, and implement them so as to be able to conduct comparisons. Then, (b) we devise a novel method for computing the Hildebrand diagram pertaining to any given simulated robot motion. Our approach (c) employs two different definitions for the motion stride, the *classical* and the *alternative* one [6], [4]. Next, (d) we explore the effects of various robot parameters to the gait the robot eventually employs, by using the simulation environment and the procedure for computing Hildebrand diagrams. Finally, (e) we attempt to provide some intuition about the steady state part (i.e., the periodic part) of the robot motion, by employing a new family of abstract patterns which are able to characterize robot motions that are not composed of a single gait only, but rather by a periodic sequence of gaits.

In general, a gait is defined such that at each stride the motion repeats itself in all detail [4]. However, there are cases at which the robot does a few strides, which are all different among them, but after this number of strides the robot is at the same *condition* as it was at the beginning of these strides. Here, we cannot speak of a gait, but for steady state patterns in which the robot locomotes. We search for these patterns in a mechanistic way — by exploiting a number of mathematical relations that emerge between the computed Hildebrand diagram components, for both the two stride definitions, and the structure of these patterns. In this paper, we expand our previous preliminary work [7] so as to include both the examination of more robot parameters, and the introduction and computation of the new aforementioned patterns. We also provide some novel results about the connection between gravity acceleration, leg rest length, as well as leg mass, and the gait that is eventually selected by the robot in its steady state.

II. Gaits and Hildebrand Diagrams

In the study of legged animals or robots, the concepts of stride and gait are very important. Stride is the part of the robot motion that is defined by any two successive touch-downs of its left hind leg. The gait is a way to categorize the stride of a given robot locomotion, by incorporating its main features about the placement of each leg and their respective touch-down and lift-off timings.

Strides and gaits can be described and analysed using Hildebrand diagrams and/ or gait graphs [4]. The format of a Hildebrand diagram, see Fig. 1, is as follows: On the vertical axis, there are four black horizontal line segments, each corresponding to a different leg. When a leg touches the ground, the respective line segment is depicted to be thick, whereas when it is on the air, this segment is depicted to be dotted. On the horizontal axis appears the % percentage of the stride duration that is completed.

*This research has been financed by the European Union (European Social Fund — ESF) and Greek national funds through the Operational Program "Education and Lifelong Learning" of the National Strategic Reference Framework (NSRF — Research Funding Program: ARISTEIA: Reinforcement of the interdisciplinary and/ or interinstitutional research and innovation.)

Dimitrios Myrisiotis and Evangelos Papadopoulos are with the School of Mechanical Engineering, National Technical University of Athens, 9 Heroon Polytechneiou Str., 15780 Athens, Greece (E-mails: dimyrisiotis@gmail.com, egpapado@central.ntua.gr; tel.: +30-210-772-1440.)

Ioannis Poulakakis is with the Department of Mechanical Engineering, University of Delaware, DE, USA (E-mail: poulakas@udel.edu.)

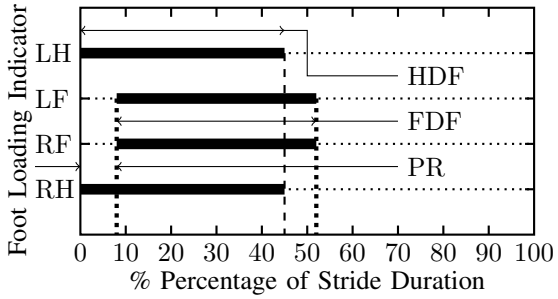

Fig. 1: A Hildebrand diagram depicting the gait that corresponds to animal or robot locomotion.

The quantities HDF, FDF and PR that appear in the Hildebrand diagrams are respectively: the hind (back) and fore (front) duty factors, and the phase relationship. Each duty factor informs us about the fraction of the stride duration the hind or fore legs touch the ground. The phase relationship informs us about the time difference, as a fraction of stride duration, between the touch-downs of the hind and fore legs.

An alternative form is the *gait graph*, see Fig. 2, in which each gait is depicted as a dot. The vertical axis shows the phase relationship (or phase) and the horizontal the mean value of the hind and fore duty factors (or mean factor.)

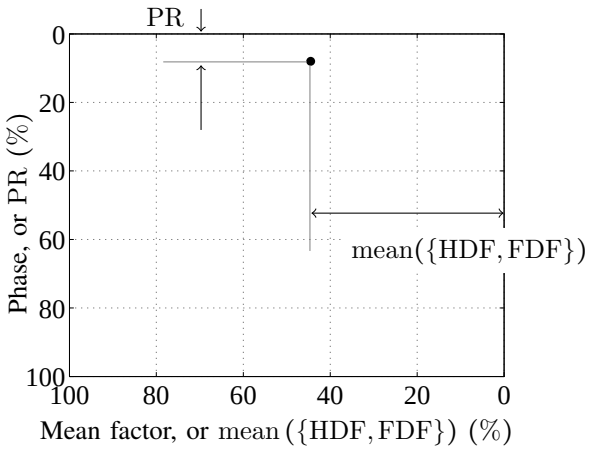

Fig. 2: The gait graph corresponding to the Hildebrand diagram of Fig. 1.

There is a vast variety of different possible gait forms. For example, whenever the hind or fore pair of legs operate in phase the gait that results is called *bound*. In the case where all the legs operate in phase, we have *pronk* [8].

III. The Quadruped Robot

A planar quadruped robot consists of a body, the hind and fore compliant *virtual legs*, or VLegs [1], and two rotational joints. A graphical illustration is depicted in Fig. 3.

Modeling. For the modeling of the quadruped robot [9], [10], [11], we employed the Euler–Lagrange method [12], [2]. Let U denote the potential energy of the robot, T its

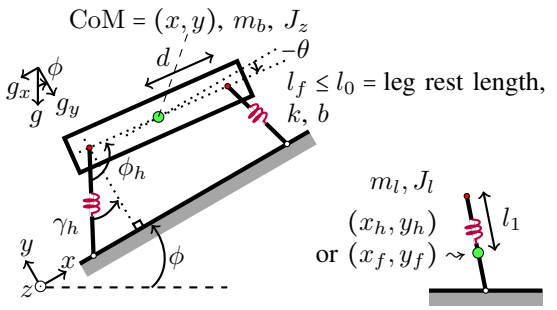

(a) The employed model of the quadruped robot depicted in the sagittal plane in uphill locomotion. The VLegs are massless.

(b) A VLeg, when considered as having mass.

Fig. 3: Robot models. Inputs: Hip torques $\tau_{z,h}$ and $\tau_{z,f}$.

kinetic energy and let t denote time. Let, also, $\dot{q} = \frac{\mathrm{d}q}{\mathrm{d}t}$, for any modeling quantity q. Using the Lagrangian

$$L = U - T \tag{1}$$

and the energy losses

$$\Delta = \frac{1}{2} b \dot{l}_h^2 + \frac{1}{2} b \dot{l}_f^2 \tag{2}$$

and, denoting by $\tau_{z,h}$ and $\tau_{z,f}$ the torques exerted at the hips of the VLegs, the power input

$$\Pi = \dot{\phi}_h \tau_{z,h} + \dot{\phi}_f \tau_{z,f} \tag{3}$$

the equations of motion are given by

$$\frac{\mathrm{d}}{\mathrm{d}t}\left(\frac{\partial L}{\partial \dot{\mu}}\right) = \frac{\partial L}{\partial \mu} + \frac{\partial \Pi}{\partial \dot{\mu}} - \frac{\partial \Delta}{\partial \mu} \tag{4}$$

where μ ranges over the appropriate, each time, set of degrees of freedom (DOFs:) since this process is implemented for two different models of the robot — according to whether the legs are considered to have mass or not.

Model A. [DOFs: x, y, θ] The Lagrangian for a robot with negligible leg mass is (see Fig. 3a):

$$\begin{aligned} L_A = {} & \frac{1}{2} m_b \left(\dot{x}^2 + \dot{y}^2\right) + \frac{1}{2} J_z \dot{\theta}^2 - \frac{1}{2} k \left(l_0 - l_h\right)^2 \\ & - \frac{1}{2} k \left(l_0 - l_f\right)^2 - m_b g \cos(\phi) y - m_b g \sin(\phi) x. \end{aligned} \tag{5}$$

Model B. [DOFs: $x, y, \theta, \phi_h, \phi_f$] The Lagrangian for a robot with legs with significant leg mass is (see Figs. 3a and 3b):

$$\begin{aligned} L_B = {} & \frac{1}{2} m_b \left(\dot{x}^2 + \dot{y}^2\right) + \frac{1}{2} J_z \dot{\theta}^2 - m_b g \sin(\phi) x \\ & - m_b g \cos(\phi) y + \frac{1}{2} m_l \left(\dot{x}_h^2 + \dot{y}_h^2\right) + \frac{1}{2} J_l \dot{\gamma}_h^2 \\ & - \frac{1}{2} k \left(l_0 - l_h\right)^2 - m_l g \sin(\phi) x_h - m_l g \cos(\phi) y_h \\ & + \frac{1}{2} m_l \left(\dot{x}_f^2 + \dot{y}_f^2\right) + \frac{1}{2} J_l \dot{\gamma}_f^2 - \frac{1}{2} k \left(l_0 - l_f\right)^2 \\ & - m_l g \sin(\phi) x_f - m_l g \cos(\phi) y_f. \end{aligned} \tag{6}$$

In the flight phase of the robot described by model B, the conservation of the angular momentum is taken into account, as it provides an integral of motion. Note that the torques exerted at the hips are quantities bounded by some function defined on foot–ground friction — according to criteria regarding foot slipping and loss of balance [13].

Dynamical Phases. The dynamical phases of our modeled robot are four: flight, hind stance, double stance and fore stance. In *flight*, every leg is on the air. In *double stance*, every leg touches the ground. In *hind stance*, only the hind VLeg touches the ground. Similarly, we define *fore stance*.

Control Philosophy. In order for our quadruped to locomote, there should be a way to sustain the energy amount required for its motion. This is accomplished by compensating the inevitable energy losses occuring at each stance phase [10]. In each stance, the hip joint motors are activated to compress the leg springs push forward the robot body — and thus to add energy to the system. So, each time the robot is on the air, the control system rotates the legs in order for these to land safely in the upcoming stride. In this way, the gaits that result are the same to those obtained by a *passive robot*, i.e., robot motion without energy losses — although here all losses are compensated for by power provided by the controlled hip motors. We note that the controller takes as inputs the desired CoM appex height and the CoM forward velocity values, thus, we can be sure that the leg tip will not collide with the ground — if one adjusts appropriately the desired CoM appex height value.

IV. Hildebrand Diagrams Computation

To generate a Hildebrand diagram, we first isolate the periodic part of the robot motion, and then we compute the quantities HDF, FDF and PR that regard the steady state part of its motion.

Transition Time Instance. We define as *steady state* the part of the robot motion that is periodic. The complement of the steady state, with respect to the total motion duration, is called *transient state*. Let t_{TtS} (i.e., *Transient to Steady*) be the time *instance* that separates the transient from the steady state part. We present an example about the nature of the time instance t_{TtS}, in Fig. 4.

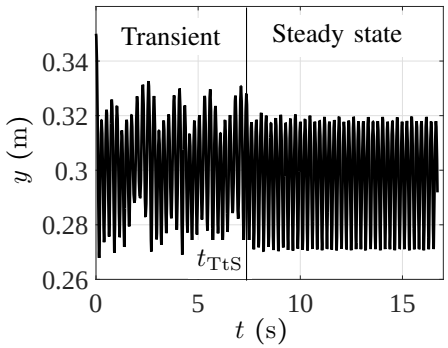

Fig. 4: Transition time instance example.

Components Calculation. The quantities that compose a Hildebrand diagram, are the quantities HDF, FDF and PR, see Figs. 1 and 2. We will employ two different definitions about the stride [4], [6]. The first is the *classical* (subscript C) definition in which the stride is defined as the part of the robot locomotion located in between of two successive touch-downs of the *hind* VLeg. The *alternative* (subscript A) definition, is that in which the stride is perceived as the part of the robot locomotion contained between two successive touch-downs of the *fore* VLeg. Let $Q \in \{\mathrm{HDF}, \mathrm{FDF}, \mathrm{PR}\}$. We denote as Q_j, with $j \in \{C, A\}$, the vectors that hold the values of the quantity Q computed according to the classical and the alternative stride definition, respectively, for all the steady state strides. For a vector V, we denote by $V[i]$ its i^{th} entry. The need for using two stride definitions comes from the fact that when using only the classical one, and the robot lands with its fore legs after a flight phase, for two consecutive flight phases, we get unrealistically large ($\geq 50\%$) PR value results, see Fig. 5, in which, for the i^{th} steady state stride, say, we get

$$\begin{aligned} \mathrm{PR}_C[i] = \frac{\alpha}{\beta} &\approx 0.95 \\ &\gg 0.05 \\ &\approx \frac{\gamma}{\delta} = \mathrm{PR}_A[i] = \text{actual phase value.} \end{aligned} \tag{7}$$

On the contrary, the values of HDF and FDF do not differ by much ($< 5\%$) when using separately the two stride definitions. For these quantities, we use only the classical.

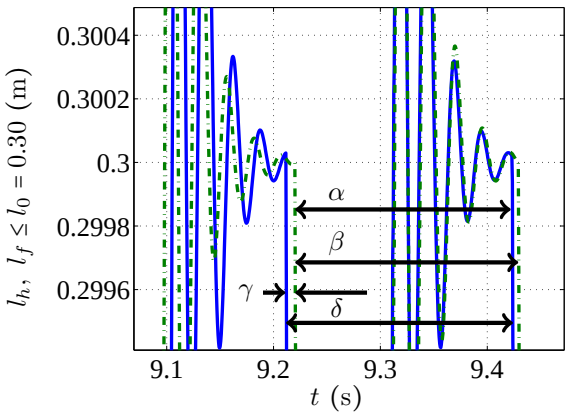

Fig. 5: Unrealistically large PR value computation when using the classical definition. The continuous line corresponds to the fore VLeg, whereas the dashed one to the hind VLeg. Note that if one interchanges the roles of the continuous and dashed lines, we get a symmetric result regarding unrealistic PR values when using the alternative definition.

Let Q and Q_j be as above, and let $q \in [0, 1)$. We define

$$q \text{ is Small} \equiv_{\mathrm{def}} q < 50\% \tag{8}$$

and

$$q \text{ is Big} \equiv_{\mathrm{def}} q \geq 50\% \tag{9}$$

and, for every $j \in \{C, A\}$, we also define

$$Q_j^{\text{Small}} =_{\text{def}} \text{the subvector of } Q_j, \text{ consisting of its Small values only.} \quad (10)$$

Finally, if we denote by "$\cup$" the vector-union operation, that allows element-repetitions, we set

$$\text{HDF} =_{\text{def}} \text{mean}\left(\text{HDF}_C\right) \approx \text{mean}\left(\text{HDF}_A\right), \quad (11)$$

$$\text{FDF} =_{\text{def}} \text{mean}\left(\text{FDF}_C\right) \approx \text{mean}\left(\text{FDF}_A\right), \quad (12)$$

$$\text{PR} =_{\text{def}} \text{mean}\left(\text{PR}_C^{\text{Small}} \cup \text{PR}_A^{\text{Small}}\right). \quad (13)$$

Steady State Patterns. We define a class of patterns that are more abstract from the concept of gait. Here, we are concerned only about the first VLeg to touch the ground, after a flight phase. For example, by "HFF" we denote the pattern that, according to which, the steady state is composed by a sequence of three strides: one that begins with a touch-down of the hind legs, and two that begin with the touch-downs of the fore legs.

Let V be some vector. By $\text{tr}\,(V)$ we denote the number of transitions from a Big to a Small value, or vice versa, in V. We introduce, in Table I, an experimentally (i.e., in MATLAB-simulations) verified comprehensive quantitative characterization of the phase vectors PR_C and PR_A.

TABLE I
PR_j VECTORS SPECIFICATIONS, FOR $j \in \{A, C\}$

Symbol	Meaning
s	The respective PR_j vector contains Small values only.
B	The respective PR_j vector contains Big values only.
sB	The respective PR_j vector contains Small or Big values.
sBo	The respective PR_j vector contains Small or Big values in an specific, alternate, fashion.

In Table II, we present a set of conditions which, when hold true, characterize the robot locomotion in terms of the pattern that abstractly describes it. Note that "NO" stands for *not observed*, and that all the other combinations of PR vectors specifications are mathematically impossible. Note, also, that for a vector V, $|V|$ denotes the number of its elements.

TABLE II
PATTERN COMPUTATION AND PORTAITURE

Pattern	Model A/B	PR_C/PR_A	Equivalent Condition
H	○/◁	s/B	$\min(\text{PR}_A) > \max(\text{PR}_C) + \tau$
F	NO/NO	B/s	$\min(\text{PR}_C) > \max(\text{PR}_A) + \tau$
HF	NO/NO	s/s	$\text{tr}(\text{PR}_C) = 0$ & $\text{tr}(\text{PR}_A) = 0$
One H	∗/▷	sB/s	$\max(\text{PR}_C) > \max(\text{PR}_A) + \tau$
One F	•/☆	s/sB	$\max(\text{PR}_A) > \max(\text{PR}_C) + \tau$
HFF	×/+	sBo/s	$\text{tr}(\text{PR}_C) = \lvert\text{PR}_C\rvert - 1$ & $\text{tr}(\text{PR}_A) = 0$
FHH	□/◇	s/sBo	$\text{tr}(\text{PR}_A) = \lvert\text{PR}_A\rvert - 1$ & $\text{tr}(\text{PR}_C) = 0$
Random	△/▽	sB/sB	Applies if no other pattern does.

But why does the condition

$$\text{tr}\,(\text{PR}_C) = |\text{PR}_C| - 1 \qquad \& \qquad \text{tr}\,(\text{PR}_A) = 0 \quad (14)$$

imply the pattern HFF? Well, the values of the PR_C are Small or Big in an alternating fashion since the number of transitions is the maximum possible, $|\text{PR}_C| - 1$. Can the values of PR_A be all Big? NO, since every Big value in PR_C is matched to two Small values in PR_A. Thus, PR_A contains only Small values. So we can identify a "FF" subpattern when encountering a Big value in PR_C, and a "HF" or a "HH" subpattern when encountering a Small value in PR_C. But identifying "HH" is impossible since there are no Big values in PR_A. All together, give the pattern "HFF." In a similar way, one can justify the conditions that lead to the rest of the patterns.

V. SIMULATION RESULTS AND ANALYSIS

Using the two proposed robot models, i.e., model A, see eq. (5), and model B, see eq. (6), the developed methodology for computing the Hildebrand diagrams, and the set of initial conditions and nominal parameter values of Table III, that are directly related to the NTUA Quadruped [11], we explore the effects of various robot parameters to the characteristic measures of the gaits followed by the robot.

TABLE III
NOMINAL PARAMETER VALUES

Symbol	Quantity	Value	Units
m_b	Body mass	9.25	kg
m_l	Leg mass (in Model B only)	0.61	kg
d	Hip joint distance	0.25	m
l_0	Leg rest length	0.30	m
k	Leg stiffness	6800.00	N/m
b	Leg dissipation coefficient	10.00	Ns/m
g	Gravity acceleration	9.81	m/s^2
ϕ	Ground inclination	0.00	rad
$\dot{x}_{\text{des}}$	Desired body CoM forward speed	1.00	m/s
h_{des}	Desired body CoM appex height	0.32	m/s
x_0	Initial body CoM height	0.35	m
$\dot{x}_0$	Initial body CoM forward speed	0.60	m/s
$\dot{y}_0$	Initial body CoM vertical speed	0.00	m/s
θ_0	Initial body CoM pitch angle	0.60	m/s
τ	Robot-specific parameter used in pattern computation	0.35	—

To explore the parameters effects, we create some *multiple gait graphs*, that is, simultaneously plotted gait graphs for many simulated motions which differ by a single value — the value of the parameter whose effects we want to examine regarding robot walking. The arrows in these figures indicate that the parameter under study is increasing along the arrow direction. The markers refer to the patterns of Table II.

Design Parameters. We investigate the significance of body mass, leg rest length and leg stiffness to the robot locomotion, using Fig. 6. We treat each parameter separately:

As shown in Fig. 6a, as the body mass increases, the mean factor is increasing from $32\% - 38\%$ to $56\% - 58\%$ for both models. The reason is that greater mass forces the legs to stay longer on the ground. However, as also shown in Fig. 6a, the phase does not change much.

Observing Fig. 6b, we have that as the leg rest length increases, the mean factor inceases from $20\% - 25\%$ to $40\% - 45\%$ for both models. This result is somewhat surprising, since longer legs can lead to greater jump-steps, and thus less ground contact, but greater leg rest length can also lead

to more frequent ground contact, for equilibrium reasons, as it is the case here. From Fig. 6b we also deduce that phase does not get affected significantly.

Fig. 6c, shows that the increase in leg stiffness reduces the mean factor from $54\% - 58\%$ to $28\% - 30\%$ for both models. This is a predictable result, since stiffer springs lead to greater axial leg forces, something that leads to less ground contact duration. Fig. 6c, also shows that the phase does not change considerably.

Control Parameters. We reveal the effects of desired appex height and desired forward speed to the robot walking behavior, using Fig. 7. We treat each parameter separately:

As illustrated by Fig. 7a, as the desired appex height increases, the mean factor decreases from $40\% - 45\%$ to $15\% - 25\%$ for both models. This is a reasonable result: The higher the robot jumps, the less time it touches the ground. The same figure shows that the phase does not change much.

Using Fig. 7b, it is quite interesting to observe that the increase in desired forward speed changes the resulting gait differently — depending on the existence of leg mass. For model A, the increase of forward speed decreases the mean factor from 46% to 32%, i.e., the leg is less time on the ground applying a torque to the body, whereas for model B, the increase of speed increases the phase from 2% to 22%, i.e., the torques are applied for longer time but not successively, and not almost simultaneously — as previously.

Environmental Parameters. Using Fig. 8, we examine the gravity and ground inclination effects to the walking behavior of the robot. We again treat each parameter separately:

By examining Fig. 8a, we note that the increase of ground inclination, increases the phase from 4% to $14\% - 16\%$ for both models. This is reasonable, since during uphill motion, there is an horizontal component of the gravitational force that pulls the robot back. Thus, it delays the touch-down of the other leg. By Fig. 8a, also, we see that the mean factor does not change much.

As shown in Fig. 8b, the increase of the acceleration of gravity increases the mean factor from $22\% - 32\%$ to $62\% - 66\%$ for both models. This is also reasonable, since greater gravity acceleration leads to greater weight forces and, thus, to longer ground contacts. As shown in Fig. 8b, the phase does not change significantly. Note that, in all of the Figs. 6 – 8, the model B curves are richer in pattern distribution — and thriftier in the size of the valid parameter-value ranges. This is due to the non-negligible leg mass: Whenever the robot is on the air, the rotation of its legs leads to the rotation of its body — as follows by the conservation of the total angular momentum. Thus, there occur more changes in the leading pair of legs at each landing of the robot. This also leads to failed simulations that regard many parameter values.

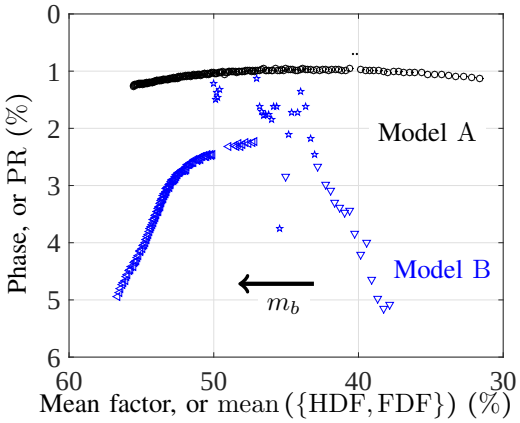

(a) Body mass (m_b) effects. Range: Model A: $4.25 - 50$ kg, Model B: $6.25 - 50$ kg.

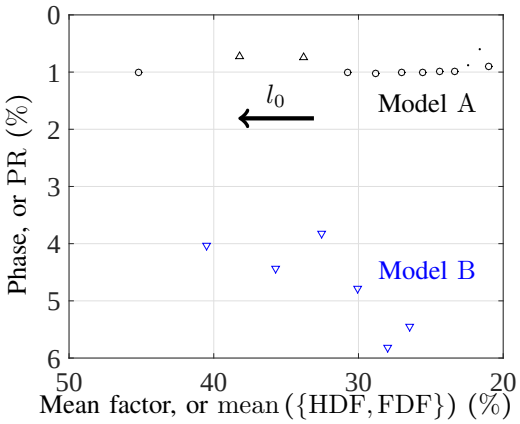

(b) Leg rest length (l_0) effects. Range: Model A: $0.20 - 0.31$ m, Model B: $0.25 - 0.30$ m.

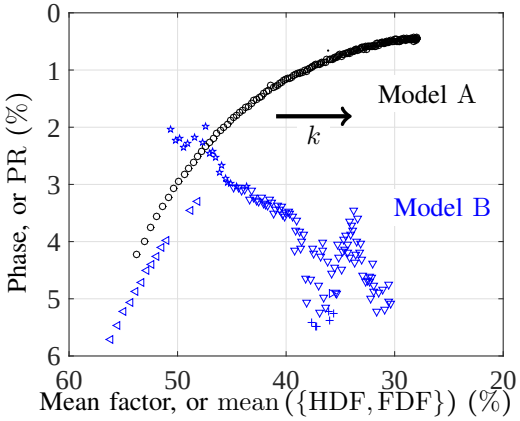

(c) Leg stiffness (k) effects. Range: Model A: $1600 - 18900$ N/m, Model B: $1900 - 16700$ N/m.

Fig. 6: Design parameters effects.

VI. Conclusion

We witnessed the exploration of the effects of the most significant robot parameters in the way a quadruped robot locomotes, and we investigated the distribution of the members of a specific pattern class. Some of our results were unknown, or not obvious. These include: (a) the connection between the leg rest length and the robot walking behavior, (b) the observation that, in general, quadruped robots modeled the way we studied, land on their hind legs after a flight phase [The pattern "H" is the most frequent,] and (c) the fact that leg mass conveys a central role to whether a quadruped

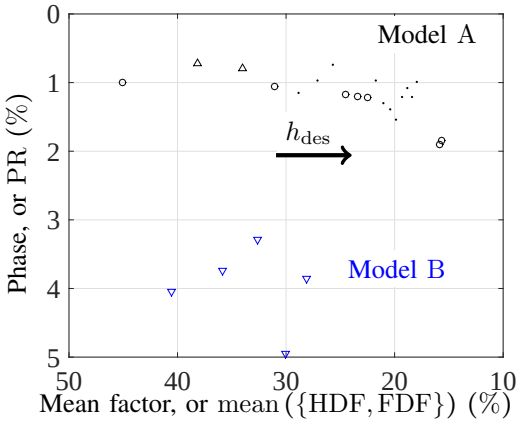

(a) Desired appex height (h_{des}) effects. Range: Model A: 0.31 – 0.68 m, Model B: 0.32 – 0.36 m.

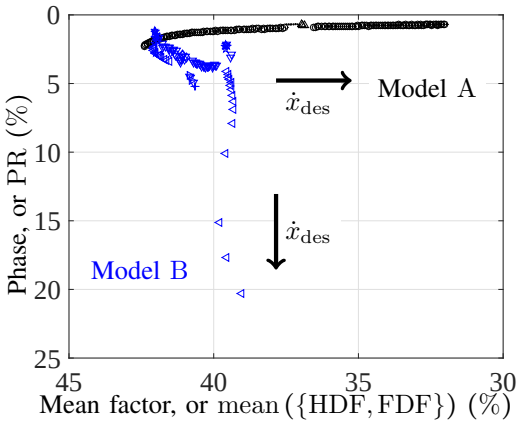

(b) Desired forward speed ($\dot{x}_{\text{des}}$) effects. Range: Model A: 0.31 – 2 m/s, Model B: 0.34 – 1.64 m/s.

Fig. 7: Control parameters effects.

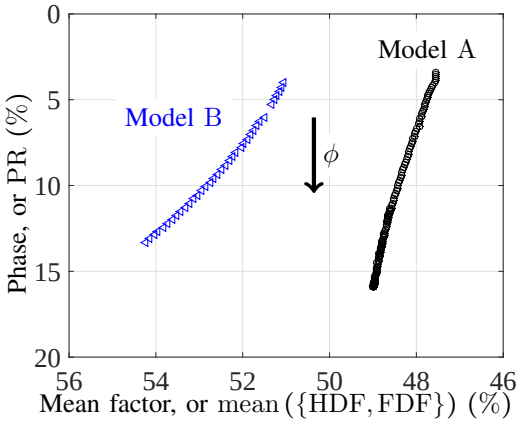

(a) Ground inclination (ϕ) effects. Range: Model A: 0 – 20 degs, Model B: 0 – 9.50 degs.

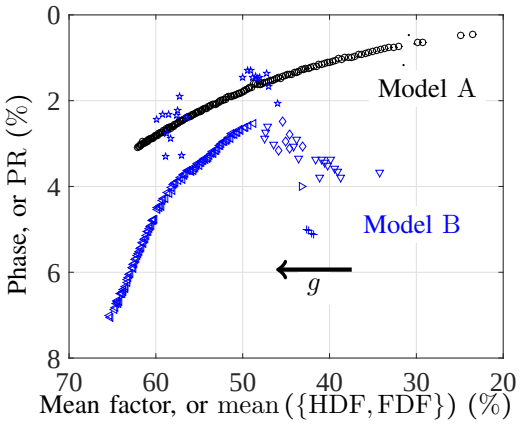

(b) Gravity acceleration (g) effects. Range: Model A: 3 – 43 m/s^2, Model B: 6 – 50 m/s^2.

Fig. 8: Environmental parameters effects.

robot will adopt a more complex locomoting pattern in its steady state. Thus, (d) we attained a qualitative view of some unexplored properties of quadruped robots, for now we can describe very concisely any quadruped robot motion. We also revealed that more complex patterns exist in legged locomotion: We discovered them, categorized them and studied the parameters that affect them. Future work includes both the derivation of algorithms that compute Hildebrand diagrams for 3D locomotion, and the expansion of the results regarding parameter effects and pattern distributions, in the 3D space, in the hope that this work will ultimately find its way to the industrial design of robots.

REFERENCES

[1] Raibert, M., *Legged Robots that Balance*, The MIT Press, Cambridge, MA, USA, 1986.

[2] Siciliano, B., Sciavicco, L., Villani, L. and Oriolo, G., *Robotics: Modeling, Planning and Control*, Advanced Textbooks in Control and Signal Processing, Springer, 2010.

[3] `http://www.bostondynamics.com/index.html`.

[4] Hildebrand, M., "The Quadrupedal Gaits of the Vertebrates," *BioScience*, Vol. 39, No. 11: *Animals in Motion*, 1989, pp. 766–775.

[5] Muybridge, E., *Animals in Motion*, Chapman and Hall, London, UK, 1957.

[6] Renous, S., Herbin, M. and Gasc, J.–P., "Contribution to the Analysis of Gaits: Practical Ways to Complement the Hildebrand Method," *Comptes Rendous Biologies*, Vol. 327, 2004, pp. 99–103.

[7] Kontolatis, I., Myrisiotis, D., Paraskevas, I., Papadopoulos, E., de Croon, G. and Izzo, D., "Quadruped optimum gaits analysis for planetary exploration," *12th Symposium on Advanced Space Technologies in Robotics and Automation (ASTRA '13)*, ESA, ESTEC, Noordwijk, The Netherlands, May 15–17, 2013.

[8] Alexander, R.–M., *Principles of Animal Locomotion*, Princeton University Press, Princeton, NJ, USA, 2006.

[9] Chatzakos, P. and Papadopoulos, E., "Parametric Analysis and Design Guidelines for a Quadruped Bounding Robot," *Proc. 15th IEEE Mediterranean Conference on Control and Automation*, June 27–29, 2007, Athens, Greece.

[10] Cherouvim, N. and Papadopoulos, E., "Speed and Height Control for a Special Class of Running Quadruped Robots," *Proc. IEEE International Conference on Robotics and Automation (ICRA '08)*, May 2008, Pasadena, CA, pp. 825–830.

[11] Kontolatis, I. and Papadopoulos, E., "Gravity and Inclination Effects on the Design of Quadruped Robots for Space Exploration," *21st Mediterranean Conference on Control and Automation*, (MED'13), Chania, Crete, Greece, June 25–28, 2013.

[12] Khalil, H. K., *Nonlinear Systems*, Prentice Hall, 2001.

[13] Kontolatis, I., Poulakakis, I. and Papadopoulos, E., "Quadruped Leg Design Principles for Handling Slopes or High-Speed Running," *ECCOMAS Thematic Conference on Multibody Dynamics*, June 29–July 2, 2015, Barcelona, Catalonia, Spain.